Integrated photovoltaic-electrochemical system for carbon dioxide reduction

Zhiwei Shen

Master of Research

School of Engineering

Faculty of Science and Engineering

Macquarie University

June 3, 2022

ACKNOWLEDGEMENTS

I would like to acknowledge my supervisor A/Prof. Yijiao Jiang for giving me the opportunity to do this work. I would like to thank my colleagues for their support. I would also like to express my gratitude to Dr. Yimin Xie for his support during the experiments.

STATEMENT OF CANDIDATE

I, Zhiwei Shen, declare that this report, submitted as part of the requirement for the award of Master of Research Degree in the School of Engineering, Macquarie University, is entirely my own work unless otherwise referenced or acknowledged. This document has not been submitted for qualification or assessment at any academic institution.

Student's Name: Zhiwei Shen

Student's Signature:

Date: 03/06/2022

LIST OF ACRONYMS

AC: Alternating current

CFP: Carbon fibre papers

CO: Carbon monoxide

CO_2: Carbon dioxide

CO_2ERR: Carbon dioxide electrochemical reduction reaction

CoPc: Cobalt phthalocyanine

CoPc/CNTs: CoPc deposited on carbon nanotubes

DC: Direct current

DMF: Dimethylformamide

FE: Faradaic efficiency

GC: Gas chromatograph

GDE: Gas diffusion electrode

$KHCO_3$: Potassium bicarbonate

KOH: Potassium hydroxide

MEA: Membrane electrode assembly

OER: Oxygen evolution reaction

PC: Photocatalysis

PS: Photosynthesis

PTFE: Polytetrafluoroethylene

PV-EC: Photovoltaic-electrochemical

STF: Solar-to-fuel

ABSTRACT

The rapid increase in carbon dioxide (CO_2) has recently become a social focus. Converting CO_2 to value-added fuels with CO_2 electrochemical reduction reaction (CO_2ERR) is an attractive method to reduce CO_2. Photovoltaic-electrochemical (PV-EC) integrated systems enable to drive CO_2ERR with renewable electricity. However, PV-EC integrated systems have different optimal conditions depending on systems configuration. The aim of this Master thesis is to design a PV-EC system with a voltage regulator component, which facilitates the system operating at the desired potential for CO_2ERR. Effects of various operating parameters were investigated. A maximum Faradaic efficiency of CO (FE_{CO}, 90%) was obtained under the optimal 1-h CO_2ERR conditions with a potential of -1.25V vs. NHE, a CO_2 flow rate of 20 mL/min, 0.5M $KHCO_3$ electrolyte in a reversely assembled flow cell. A stable FE_{CO} of ca. 95% was reached for a 4-h long electrolysis under the optimal conditions. When the electrolyser was driven by a silicon solar cell under the identical conditions, a FE_{CO} of 57% was achieved. The drop in FE_{CO} can be explained by the energy loss in between the PV and EC components. This thesis gives an insight to further improve PV-EC systems to be stably operated under optimal conditions.

Contents

List of Figures

Chapter 1 Introduction

The carbon dioxide (CO_2) concentration in the atmosphere has risen rapidly. It attracted widespread concern since CO_2 is a greenhouse gas, meaning its emission causes climate disruption. However, these emissions cannot be inevitable to some extent due to human activities such as fossil fuel combustion and changes in land use. Fortunately, the excessive CO_2 emissions can be artificially reduced. There are two common strategies to mitigate CO_2 emissions: improving the energy efficiency of fossil fuels and preventing deforestation or creating CO_2 sinks with reforestation [1]. However, both strategies have a limited impact on the reduction of CO_2 emissions and require significant investment [1, 2]. Therefore, emerging technologies of greenhouse gas capture and utilisation are in demand. Various end-of-pipe technologies have been developed to remove CO_2 from flue gas streams, including physical absorption, chemical solvent stripping, membrane separation, cryogenic separation and physical adsorption [2, 3]. The chemical absorption technology is the most reliable one because of its low degradation, minimal toxicity and regenerative capability, and it can be applied in a large-scale plant .[2, 4] However, the process is expensive and energy-consuming.

After the CO_2 is captured, it is crucial to store and utilise the CO_2 [5]. Converting CO_2 into value-added chemicals is a significant utilisation route, in which about 500 Mt/year of CO_2 can be sequestrated [4]. The production of chemicals and fuels through sustainable processes offers great benefits within the energy sector. Also, fossil fuel consumption has dropped because of the generation of chemicals and fuels by CO_2 conversion [4].

During the CO_2 reduction reaction process, CO_2 can be converted into different chemical products that depend on the applied electrocatalysts and operational conditions. Among the possible products as shown in Table 1.1, carbon monoxide (CO) has great potential in practical applications since it can be readily converted into fuels and value-added chemicals *via* the Fischer-Tropsch process [6-8]. In addition, it is one of the most accessible products to obtain since it requires only 2 electrons and two protons. There are many different methods to reduce CO_2. Photosynthesis (PS) and

photocatalysis (PC) drive chemical reaction by light energy. The photoelectrochemical method uses photoelectrodes in the electrochemical cell to drive the reaction by the photogenerated charge carriers. Photovoltaic-electrochemical (PV-EC) method consists of photovoltaic cells and electrochemical cells as an integrated system. PV component converts the solar energy to electricity, and then the PV-EC system uses the generated electricity to reduce CO_2 to CO in the EC component. Among these CO_2 reduction reaction methods, PV-EC is considered the most advanced and most promising because PS and PC's solar-to-fuel (STF) efficiency is relatively low compared to the other two methods [9]. Moreover, in PV-EC, compared to PEC, each component in PV-EC can be upgraded independently by separating the integrated system into subsystems. This facilitates system optimisation and scaling up. Most importantly, the PV-EC system is more promising because renewable electricity is used in PV components to generate electricity, and then it is used for CO_2ERR. Thus, PV-EC is the preferred method for CO_2 reduction reaction.

Table 1.1 CO_2 reduction reaction at different potentials in aqueous solution (pH=7.0)[10]

Reactions	Potential (V)
$CO_2 + e^- \rightarrow CO_2^-$	-1.9
$CO_2 + 2H^+ + 2e^- \rightarrow HCOOH$	-0.61
$CO_2 + 2H^+ + 2e^- \rightarrow CO + H_2O$	-0.52
$2CO_2 + 12H^+ + 12e^- \rightarrow C_2H_4 + 4H_2O$	-0.34
$CO_2 + 4H^+ + 4e^- \rightarrow HCHO + H_2O$	-0.51
$CO_2 + 6H^+ + 6e^- \rightarrow CH_3OH + H_2O$	-0.38
$CO_2 + 8H^+ + 8e^- \rightarrow CH_4 + 2H_2O$	-0.24
$2H^+ + 2e^- \rightarrow H_2$	-0.42

Chapter 2 Literature review

2.1 Solar cells used for CO_2 electrochemical reduction reaction (CO_2ERR)

Silicon-based, perovskite and triple-junction are the three primary types of solar cells used in PV-EC. These solar cells can produce different electrical efficiency, which is the capability of solar cells to convert solar energy to electrical energy, due to their material properties. Silicon-based solar cells are a kind of commercial solar cells that have been well developed and widely used. The rapid growth of electrical efficiency of perovskite solar cells in recent years and the ease of manufacturing make them considered to have the potential for having higher electrical efficiency.[11] Triple-junction solar cells are currently the best-performing solar cell on the market, and the electrical efficiency is the highest among these three mainstream solar cells. However, the three types of solar cells have some disadvantages. Due to extensive research on silicon-based solar cells, the development of their electrical efficiency has almost reached its peak. Perovskite solar cells also have a concern about the stability of long-term operation. Also, perovskite solar cells consist of toxic metals that would cause environmental pollution.[12] The shortcomings of triple-junction solar cells are expensive and difficult to manufacture. Scientists still need to further improve these three primary solar cells to achieve a better overall performance of solar cells.

On the other hand, STF efficiency is not only affected by solar cells but also by electrochemical cells. CO_2ERR can proceed under either batch or flow condition. The batch condition means that CO_2 is fed into the reaction cell before starting CO_2ERR, and there is no additional gas flow into the system during the reaction. In contrast, CO_2 continuously flows into the reactor system during the reaction under flow conditions. Also, the flow condition supports higher current densities because of better mass transfer of the cell, lower resistance and lower potential.[13, 14] Thus, flow condition is selected for CO_2ERR. The two primary cells used for CO_2ERR under flow conditions are H-cell and membrane electrode assembly (MEA). An H-type cell is a gas-tight glass

electrochemical cell that consists of two compartments. An MEA is a setup composed of two flow channels that allow the anolyte and catholyte to flow separately in one of these channels, and an ion-exchange membrane is used to separate the anolyte and catholyte. The MEA can improve the CO_2 reduction performance by changing the condition in the cell by comparing it with H-cell. Therefore, MEA will be the priority of the electrochemical cells for CO_2ERR in the future.

It is essential to convert solar energy into useful chemical products to ensure society's clean and renewable energy sources. Renewable energy, particularly solar energy, is increasingly adopted to optimise the safety of energy supply and improve the environmental effect of energy consumption and production, which is carbon-based as well. Solar cells can be used to produce electricity with solar energy, and then provide the electricity to an electrolyser to convert CO_2 into different chemicals. Compared to other electrochemical reduction reactions, CO_2ERR can convert CO_2 to CO, formate, and ethylene while decreasing the exhausted CO_2.

The commonly used commercial solar cells in the market for CO_2ERR are silicon-based solar cells, perovskite solar cells and triple-junction solar cells. All these solar cells will be discussed in the following subsections.

2.1.1 Silicon-based solar cells

Polycrystalline silicon solar cells are currently the market's mainstream type of solar cells. They accounted for 90% of the market share. Crystalline silicon is a material having outstanding stability and durability. In addition, the energy gap of crystalline silicon is 1.12 eV, which makes it almost the most suitable choice for maximum single-junction solar cell efficiency.[15] Silicon-based solar cells were used as the PV component. The performance of silicon solar cells is summarised in Table 2.1. For example, Lee et al. [16] reported an STF efficiency of 12.1%, lasting 5 h with commercial interdigitated back contact silicon solar cells, which has a high STF efficiency while also stable.

Table 2.1 Summary of STF of CO_2ERR for CO production using silicon-based solar cells

Electrocatalyst	Electrolyte	FE (%)	Duration (h)	η_{STF} (%)	Ref
Carbon-supported tungsten-seed-based 3D silver dendrite	0.5M $KHCO_3$	95	5	12.1	[16]
Nanoporous silver	0.5 M $NaHCO_3$	75.9	2	6.4	[17]
Ag	0.1 M $KHCO_3$ (catholyte) / 1 M KOH (anolyte)	93	8	8.0	[18]
Nanoporous silver	0.5M $NaHCO_3$	/	1	5.52	[19]
Mn-complex polymer	0.1 M mixed aqueous solution of potassium borate and sulfate	/	3	3.4*	[20]
Porous silicon and nitrogen co-doped carbon nanomaterial	0.1 M $KHCO_3$ added with 0.4 M KCl	89	2.5	12.5*	[21]
WSe_2 nanoflakes	ionic liquid 1-ethyl-3-methylimidazolium tetrafluoroborate+deionized water (vol% 1:1) (catholyte) / 0.071M Potassium Phosphate (anolyte)	24	100	4.6	[22]
Zn	0.5M $KHCO_3$ (catholyte)/ 1M KOH (anolyte)	85	10	4.26	[23]
Ag nanoparticles	0.1 M $KHCO_3$	90	3	0.1	[24]

* The η_{STF} here is solar-to-chemical efficiency, which means the efficiency of solar energy for all types of products

As shown in Figure 2.1a, a silicon solar module is directly connected with a zero-gap assembly of electrolyser to construct the large-scale PV-EC system. The silicon solar module consists of several solar cells ranging from 3 to 6, depending on the characterisation of their I-V curves, to optimise their PV module. The dimensions of the solar module are 10 cm × 12 cm. The electrical efficiency of their PV module was about 18% when the module was connected directly with their electrolyser. In order to improve the STF efficiency, instead of a carbon paper coated with IrO_2 and 0.5M $KHCO_3$, Fe-doped Co foam and 1M KOH were chosen as the anode and anolyte, respectively. It was found that the pH values of the anolyte have an important role in the overpotential of oxygen evolution reaction (OER). Compared to carbon paper, Fe-doped Co foam has high catalytic activity for OER under alkaline conditions and also has a porous 3D structure that is suitable for electrolyte transfer. Hence, the overpotential of OER under alkaline media became lower, resulting in the decrease of cell voltage of the zero-gap assembly of electrolyser. Under air mass (AM) 1.5G, 100mW/cm^2 simulated illumination, the FE was stable at over 95 % for 5 h of operation with the carbon-supported tungsten-seed-based silver dendrite catalyst. From Figure 2.1b, the FE_{CO} fluctuated around 95 %, while the current density kept decreasing during the CO_2ERR. After 5-h electrolysis, the STF efficiency was about 90 %.

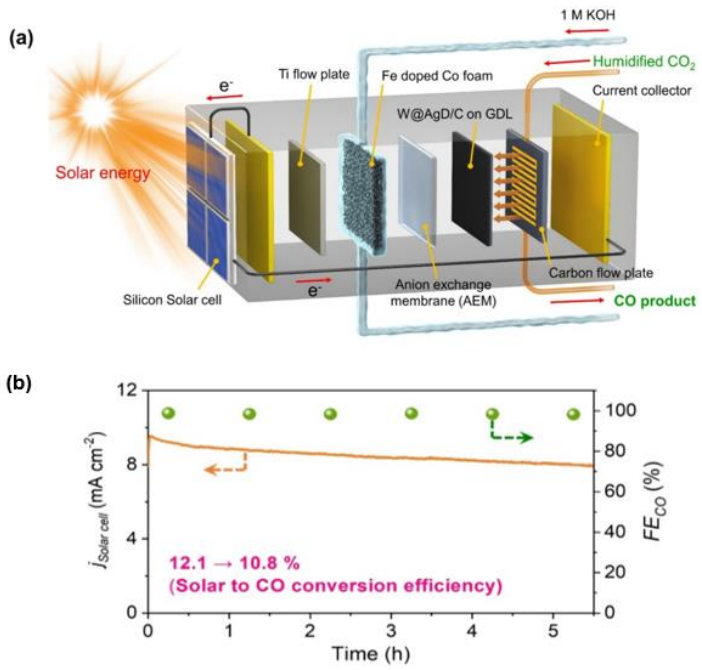

Figure 2.1 (a): Schematic of PV-EC system consists of 120 cm^2 silicon solar cell, carbon-supported tungsten-seed-based 3D silver dendrite on 10 cm^2 GDL cathode; Fe doped Co foam anode; 1 M KOH electrolyte; and anion exchange membrane. (b): FE_{CO} (green dots) and current density (orange line) of PV-EC system. [16]

Asadi et al. achieved 100 h of stability with 4.6 % STF efficiency using two series-connected amorphous silicon triple-junction solar cells.[22] The maximum electrical efficiency of this solar cell is approximately 6 %. The a-Si silicon solar cells can operate continuously for 5 h. After 5 h, the corrosion of the indium tin oxide layer on the anode stops operation, but this can be restored by replacing new solar cells. In the experiment, the a-Si solar cells were changed every 4 h and operated the CO_2ERR for 100 h in total. In addition, the FE was 24 % when using tungsten diselenide nanoflakes catalyst.

Many reliable and low-cost silicon-based solar cells have been commercially available.[17] These solar cells can supply the required current and voltage by changing their configurations. In order to optimise the voltage, the number of solar cells connected in series can be changed. Similarly, the number of cells connected in parallel can be adjusted to optimise the voltage. However, the overall STF efficiency of the silicon-based solar cells driven CO_2ERR system is still relatively low, around 4 % to

8%. It is noted that the electrical efficiency of silicon-based solar cells has almost reached its peak. Therefore, researchers have invented other types of solar cells to reach a better electrical efficiency.

2.1.2 Perovskite solar cells

Perovskite solar cells have attracted widespread interest in the past decade. The power conversion efficiency experienced a sharp increase from 3.8 % in 2009 to 23.3 % in 2018, which is comparable to the performance of commercial multicrystalline silicon solar cells [11]. Thanks to the low cost and easy fabrication of perovskite solar cells,[11, 25] they were used as the PV component in the PV-EC system, as shown in Table 2.2. For example, Esiner et al. [26] reported CO_2 reduction to CO and CH_4 using p-i-n double-cation lead halide perovskite solar cells. The solar-to-CO efficiency achieved more than 8 %, lasting 4.5 h using a gold catalyst. Since halide perovskite solar cells usually provide a voltage of around 1 V at an open circuit, solar cells need to be connected in series or stacked in a multiple-junction configuration to offer sufficient voltage to drive CO_2ERR.[26] Three series-connected planar p-i-n metal halide perovskite solar cells were used as the PV component of the CO_2ERR system. A power conversion efficiency of 17.4 % was achieved. This photovoltaic module was illuminated with AM1.5G light and 100 mW/cm^2 intensity. An STF efficiency of over 8% was obtained for the first 280 minutes using gold cathode, which is the highest STF efficiency among the CO_2ERR devices using perovskite solar cells.

Table 2.2: Summary of STF for CO_2ERR for CO production using perovskite solar cells

Electrocatalyst	Electrolyte	FE (%)	Duration (h)	η_{STF} (%)	Ref
Au	1 M $KHCO_3$	>80	4.5	>8	[26]
Au	0.5 M $NaHCO_3$	85	18	6.5	[27]
ZnTe+Au nanoparticles	0.5 M $KHCO_3$	80	3	0.35	[28]

The FE_{CO} presented in Figure 2.2a started at a very high value, greater than 90%, and then eventually decreased to around 70 % after 600 min. As a result, the STF efficiency of CO also had a sharp drop compared to the peak STF efficiency shown in Figure 2.2b. The decreased FE_{CO} might be due to the poisoning of CO product on the active sites on the gold electrode. Consequently, the operating voltage of the PV-EC system would increase, resulting in the greatly increased H_2 yield. It was also reported that a flow cell can greatly improve the CO_2ERR performance. For example, compared to H-cell, the local pH and diffusion in flow cells can be adjusted to enhance the efficiency of CO_2ERR. In addition, the distance between cathode and anode can be minimised in the flow cell leading to less resistance. Furthermore, the reactor system must be operated at a fixed potential range for H-cell to maintain a high selectivity to CO. While for a flow cell using GDE, it is feasible to change the current densities in a wide range to achieve a high selectivity to CO.

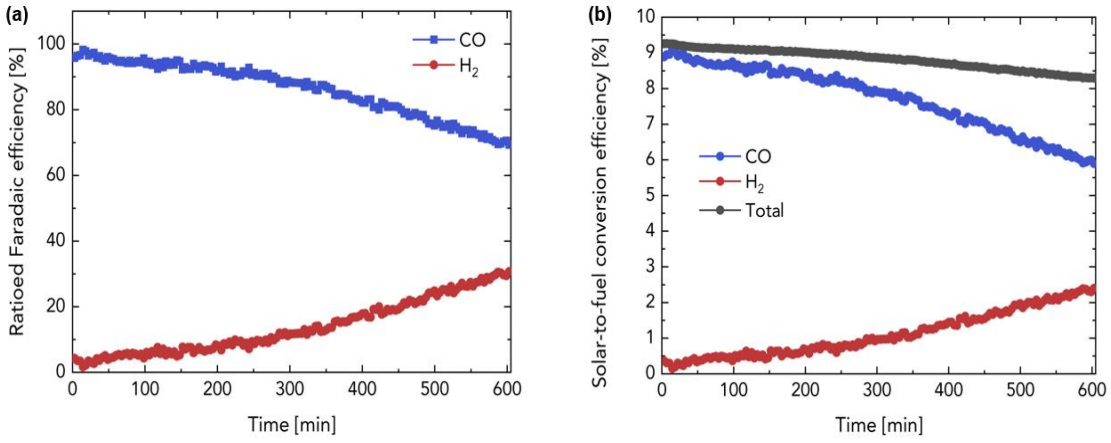

Figure 2.2 (a) FE (b) STF efficiencies of CO and H_2 of the solar-driven CO_2ERR.[26]

Similarly, Schreier et al. [27] reported an STF of 6.5% for a duration of 18 h. Three series-connected $CH_3NH_3PbI_3$ perovskite solar cells were used to drive CO_2ERR with the gold catalyst. This configuration provided an electrical efficiency of 13.4 %. The PV module was placed in a chamber fed by argon with a constant flow rate under the simulated solar illumination (AM1.5G, 100 mW/cm^2). The system drove CO_2ERR without any external bias after the electrocatalyst and PV module reached the initial equilibration. The FE varied in the range of 80 % to 90 % during the long-term operation. The main

advantage of perovskite solar cells is their high open-circuit voltage. This results in fewer perovskite cells required to provide sufficient voltage for CO_2ERR compared to conventional solar cells such as Si. Jang et al. [28] used one $CH_3NH_3PbI_3$ perovskite solar cell connected with the ZnO@ZnTe@CdTe-Au photocathode in series. Under the AM1.5G, 100W/cm^2 illumination, the system produced an STF efficiency of 0.35% for 3 h using gold electrocatalyst. The power conversion efficiency is 16.3 %.

However, perovskite solar cells also have limitations such as relatively lower performance compared with silicon-based solar cells and instability under high temperature and humidity conditions.[29]

2.1.3 Triple-junction solar cells

To achieve high electrical efficiency and stability, triple-junction solar cells are considered as one of the most commonly used solar cells as the PV component of CO_2ERR system. The solar energy conversion efficiency of a commercial GaInP/GaInAs/Ge triple-junction cell is 37.9 % [30].

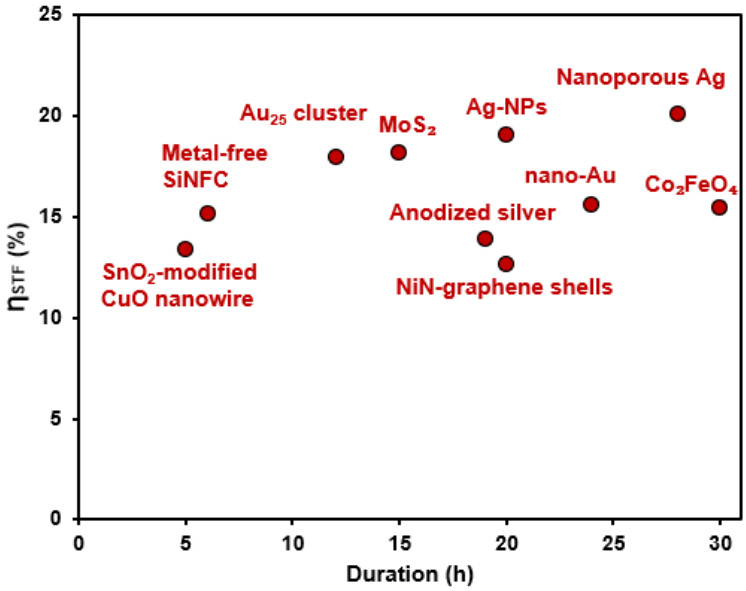

Figure 2.3 Reported STF efficiencies for PV-EC systems using triple junction solar cells with AM 1.5G simulated light.[31, 30, 32-39]

The STF efficiencies of the PV-EC systems using triple junction solar cells are depicted in Figure 2.3. Xiao et al. [34] reported the highest STF efficiency of 20.1 % over 28 h using GaInP/GaInAs/Ge triple-junction cell. It is known that commercial solar cells

usually have a flat working zone when their current densities are close to the maximum. However, the current densities out of this zone have sharp drops while the voltage increases. Therefore, the ideal working zone for the solar cells is the flat zone rather than the maximal power output point. This flat zone can provide a higher output voltage to the electrolyser than the actual potential required for CO_2ERR. The high voltage from the solar cells makes the PV-EC systems have a nearly maximal STF efficiency. The GaInP/GaInAs/Ge solar cells can provide a current density of 15.2 mA/cm^2 in the region of 1.34 to 2.20 V. In addition, these cells are the highest output voltage among all commercial solar cells.

Compared to GaInP/GaInAs/Ge solar cells, Si and perovskite solar cells can only supply lower output voltages. Typically, Si and perovskite solar cells are connected in series to afford sufficient power output to drive CO_2ERR. However, by connecting the solar cells in series, the current densities will be decreased, leading to a lower STF efficiency. There are two basic requirements for the electrolysers to fully utilise the photocurrent provided by the solar cells and maximise the STF efficiency. First, lower overpotentials used in the electrolysers enable the solar cell to operate stably under the optimal working zone. Second, in the region with 100% FE, the current densities in the electrolysers need to keep more significant than that of the optimal working zone of the solar cells. However, even the best catalysts for CO_2ERR cannot meet these three requirements, which means the photocurrent provided by the solar cells cannot be fully utilised. As shown in Figure 2.4, the STF efficiency with GaInP/GaInAs/Ge is almost 1.5 and 2.5 times the STF efficiency of perovskite and silicon solar cells, respectively. It is clear to see that Ga-based solar cells significantly improved the STF efficiency.

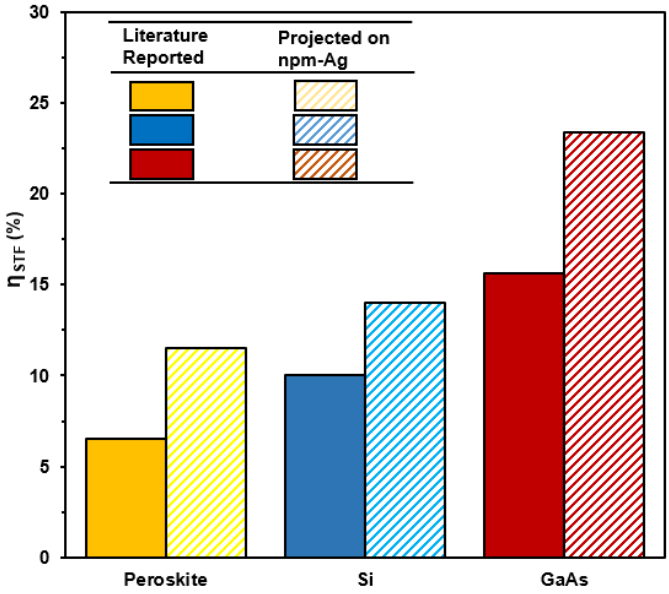

Figure 2.4 STF efficiency with different types of solar cells under AM 1.5G sunlight and electrochemical cell with GDE [34], [27], [40], [30]

Cheng et al. [31] also performed CO_2ERR using a similar PV-EC configuration using GaInP/GaInAs/Ge triple-junction cell, showing that SFE reaches 19.1 % over 20 h. Surprisingly, when the illumination intensity was changed from 1 sun to 3.25 sun, the STF was stable at 18.9 % over 150 h.

Compare all these three types of solar cells. The FE_{CO} from Esiner et al. [26] using perovskite solar cells are close to those FE_{CO} using the silicon-based solar cells. However, the STF efficiencies obtained from those two cells are not as high as that from Ga-based solar cells. Therefore, Ga-based solar cells are considered the best choice as photovoltaic cells for the PV-EC system.

2.1.4 Other solar cells used for CO_2ERR

Other solar cells have also been used for CO_2ERR. Sacco et al. [41] reported an integrated system with a dye-sensitised solar cell and an electrochemical cell. Instead of connecting the solar cell with an electrolyser externally, the integration of the PV module and electrolyser was based on a common Pt-based electrode. The Pt-based electrode was either the cathode for the PV module or the anode of the electrolyser. The PV module consists of 5 series-connected dye-sensitised solar cells. Under simulated illumination of AM 1.5G at 100mW/cm^2, the STF efficiency was 0.97 % lasting 3 h,

while the current density was stable at 6.5 mA/cm^2 after 30 min. With the Cu-Sn electrocatalyst, the intergrade system offered a FE of 78%.

2.2 Electrochemical cells used for CO_2ERR

2.2.1 H-cell

A scheme of H-cell is presented in Figure 2.5, which is a gas-tight electrochemical cell with two compartments. These cells have a limitation of mass transfer at high current densities because of the low solubility of CO_2 in water.[42]

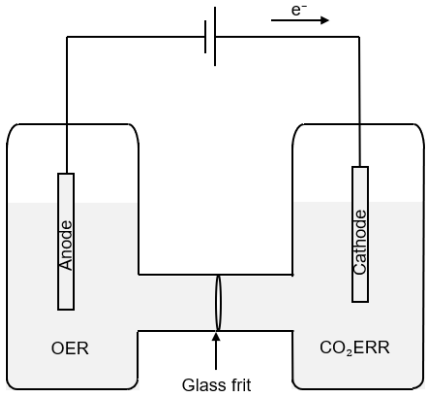

Figure 2.5 Scheme of H-cell with the electron transfer

A high STF efficiency of 15.5 % was achieved for 30 h using a triple-junction solar cell and an H-cell. by Mi et al. [37]. The solar cell was under simulated light (AM 1.5G) of 100mW/cm^2. In the H-cell, the cathodic and anodic compartments were separated by a bipolar membrane, allowing the catholyte and anolyte to operate at steady-state pH values [43], [44]. The electrolyte used for both compartments was CO_2 saturated 0.1M $KHCO_3$. Both the cathode and anode used Co_2FeO_4 nanosheet arrays as the bifunctional electrocatalyst. This electrocatalyst resulted in less polarisation and kinetic overpotential losses during CO_2ERR. The area of both cathode and anode were set as 1 cm x 1 cm. With this configuration, an average FE of 92.3% was obtained at the current density of 13.1mA/cm^2.

Zhou et al. [36] used triple-junction GaInP/GaInAs/Ge solar cell and H-cell for CO_2ERR. An STF efficiency of 13.9 % was achieved for 19 h using the triple-junction solar cell

with a maximum electrical efficiency of 28.5 % under simulated light (AM 1.5G, 100mW/cm^2). The bipolar membrane (BPM) allows the CO_2ERR to be operated at various pH values and easy gaseous product separation. However, it will result in possible potential losses as well as make the optimisation of electrochemical cells more complicated [17], [45], [46]. Besides, the ion crossover induced by BPM has to be solved for long-term operation [32]. Instead of a bipolar membrane, Nafion 117 membrane was used to separate the two compartments of the H-cell. In Zhou's work [36], the fluctuation of current density and voltage was less than 6 % and 3 %, respectively, proving the stability of a BPM-free reactor system using the Ag cathode for CO_2ERR and CO_2 saturated 0.1 M $NaNO_3$ as the electrolyte. An average FE of 87 % to 89 % was achieved during a 19-h long-term electrolysis.

Ghausi et al. [21] reported that the H-cell was employed for both CO_2ERR and OER using porous silicon and nitrogen co-doped carbon as a bifunctional electrocatalyst. A Nafion membrane was used to separate the two electrodes. The electrolyte was 0.1 m $KHCO_3$ added with 0.4 m KCl. Under simulated light (AM 1.5G, 100mW/cm^2), the integrated system of a polycrystalline Si solar cell (max electrical efficiency: 16.6%) and the H-cell has a solar-to-all product efficiency of 12.5 % for 150 min. The FE_{CO} was 89 %.

2.2.2 Continuous flow cell

Compared to H-cell, flow cell has less electrical resistance in the circuit when it is connected to the PV-EC system and can achieve higher current densities and higher STF efficiency. Cheng et al. [31] used a flow cell with a gas diffusion electrode (GDE) that reached an STF efficiency of 19.1 % lasting 20 h. Due to the low solubility of CO_2 in water (33.4mM), restricted operating pH values (~6-10) and slow ionic transfer occurred in the aqueous electrolyte, leading to high overpotentials. The use of GDE in the electrochemical cell can overcome these limitations and result in lower overpotentials and higher current densities.[47-53] The use of GDE in the electrochemical cells accompanied by a humidified gas feed into the cell makes better ion conduction and water balance. Moreover, GDE assemblies are more suitable for high current densities since salt precipitation or membrane dehydration in membrane electrode

assemblies (MEA) decreases the stability at high current densities [54]. Hence, aqueous GDE assembly was used to directly connect with triple-junction solar cells. A relatively low load of Ag electrocatalyst (0.12 mg/cm^2) on GDE was applied to match the lower current densities of solar cells. It was found that aqueous GDEs have an issue of flooding or saturation of porous catalyst layer with electrolyte, resulting in a thick layer of electrolyte (>1μm) that limited the CO_2 diffusion to the electrode. Therefore, a different method was used to set up the GDE assembly as shown in Figure 2.6, in which the electrocatalyst layer faced away from the electrolyte and towards the CO_2 supply. The reverse assembled GDE avoid the electrocatalyst layer being flooded. The anode was Ni foam, and the electrolyte was 1M KOH. An anion exchange membrane was used to separate the cathodic and anodic compartments. With the same initial current densities, the FE decreased to 50 % using the standard assembly after 2 h and 97 % with the reversed assembly after 3 h. It appeared that the electrocatalyst layer was flooded after 1 h of the operation in the standard assembly. The integrated system with the reversed assembly and triple-junction solar cells is shown in Figure 2.6. The system achieved an STF efficiency of 19.1 % for 20 h under AM 1.5G illumination at 100mW/cm^2. Moreover, this system reached an STF efficiency of 18.7 % under outdoor conditions during midday.

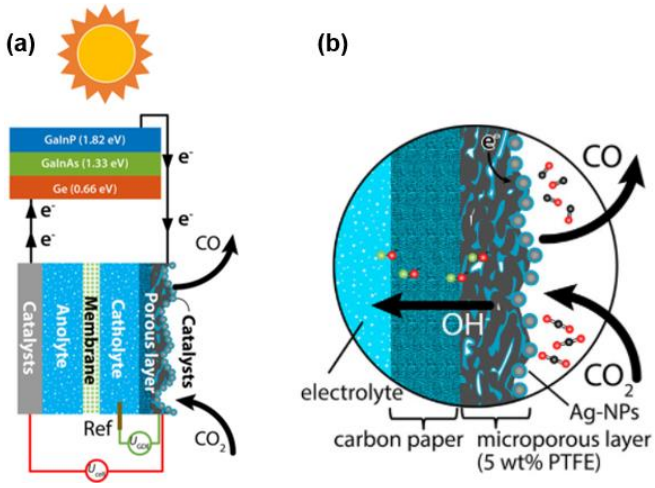

Figure 2.6 Scheme of integrated PV-GDE system (a) and the reverse assembled GDE (b).[31]

Lee et al. [16] also used commercial silicon-based solar cells, and a zero-gap assembly of electrolyser reached an STF efficiency of 12.1 % for 5 h. MEA was used in the electrochemical cell with an active surface area of 10 cm^2. The flow channel was serpentine in the cathodic compartment while it was pin shaped in the anodic compartment. Humidified CO_2 was fed to the cathodic compartment at 70 ℃, which was heated up by a heating mantle, and 0.5M $KHCO_3$ flowed into the anodic compartment by a pump. The system exhibited a FE of 95 % in the solar-driven CO_2ERR using carbon-supported tungsten-seed-based 3D silver dendrite.

2.3 Coupling methods of PV-EC systems

After the equipment of the PV-EC systems has been selected, the next important step is to choose a suitable coupling method. Sriramagiri et al. studied the effect of coupling methods on the PV-EC performance.[19] The PV component's current-voltage characteristics are highly dependent on the insolation and operating temperature, while the output of the PV component will not change with the atmospheric conditions. Consequently, it is crucial to ensure the electricity transfer between the PV module and electrolyser is stable at its maximum power output point. As shown in Figure 2.7, three coupling methods can be used for PV-EC systems: direct coupling, direct current (DC)-DC coupling, and DC-alternating current (AC)-DC coupling. DC-DC coupling uses a DC-voltage regulator with maximum power point tracking to convert the DC voltage output of the PV module into another DC voltage level for the electrolyser. This device converts the PV output voltage into the voltage at the maximum power point on the I-V curve. DC-AC-DC coupling uses a PV inverter with a maximum power point tracking function to convert the DC voltage output at the maximum power point of the PV module into AC voltage for the electrolyser designed for AC (grid). Sriramagiri reported a switch-mode DC-voltage regulator with maximum power point tracking used between the PV module and electrolyser enabled to obtain an optimal electricity transfer within the PV-EC system under fluctuating insolation. This regulator will keep changing the operating voltage of the PV module so that the PV module can maintain its maximum power point with variable insolation and temperature, then provide an

optimal voltage and current to the electrolyser. The maximum power point tracking and V/I regulation function are similar to charge controllers, which have been widely used to charge PV batteries.

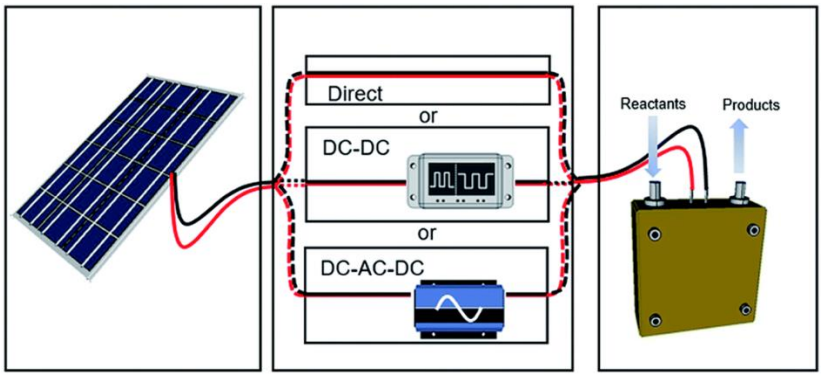

Figure 2.7 Schematic of a PV-EC system with three different coupling methods [19]

Another coupling method is an inverter-connected PV module to electrolyser designed for AC to optimise the electricity transfer (noted as DC-AC-DC in Figure 2.7). This method also ensures maximum electricity transfer except for additional losses involved in converting AC power back to DC in the electrolyser, as all PV inverters provide maximum power point tracking on their DC input side. In addition, another significant practical value is to allow the PV module to directly provide energy to the grid or the electrolyser or both in parallel.

There are several practical advantages of indirect PV-EC coupling methods. First, it can get a tunable ratio of H_2 and CO produced from the electrolyser caused by the different intensities of sunlight. Second, the ratio of CO and H_2 is adjustable for the downstream Fischer-Tropsch process. Third, the electrolyser and grid-connected PV modules can operate simultaneously. Fourth, it prevents the I-V curve of the electrolyser from shifting downwards, resulting in the maximum power-output point and coupling efficiency change over time. The indirect coupling method alleviates the problems caused by the degradation of the electrolyser and PV module. Moreover, a megawatt-scale PV-EC system was used when the system did not match its optimal power for direct coupling. The product yield of indirect coupled PV-EC would be many times higher than that of the direct-coupled systems.

Chapter 3 Experimental methods

3.1 Catalyst preparation

All the chemicals used were purchased from Sigma Aldrich. First, 2 mg cobalt phthalocyanine (CoPc) was dissolved in 10 mL dimethylformamide (DMF). Then, the CoPc solution was sonicated for 1 h. Meanwhile, a given amount of carbon nanotubes (CNTs) with a ratio of CoPc to CNTs of 3:37 was dispersed in 20 ml DMF under sonication for 1 h. The CoPc solution was then mixed with the CNTs suspension. The mixture was sonicated for another 30 min and then stirred for 24 h at room temperature. Afterwards, distilled water was added to the above mixture for the precipitation of CoPc. The mixture was centrifuged and washed with ethanol for three times. Then the material was dried under vacuum for 24 h. For a typical procedure to prepare the catalyst ink, 1 mg catalyst was dissolved in 2 mL ethanol followed by adding Nafion (5 wt. % in lower aliphatic alcohols and water) to achieve an amount of 50μL in 1mL catalyst ink under sonication for 1 h.

3.2 Electrode preparation

The electrodes used in all the experiments were polytetrafluoroethylene (PTFE) treated carbon fibre papers (CFP). First, the CFP electrode was cut into a circle with a diameter of 8 mm. It was then dried at 80°C. The CoPc/CNTs ink in ethanol was drop-casted on the CFP electrode. The final catalyst concentration on the CFP electrode is 1 mg/cm^2. The drop casted CFP electrode was dried at 80°C overnight to ensure the complete removal of ethanol.

3.3 Electrochemical experiments

For electrochemical experiments, a Biologic SP-300 potentiostat was employed. All the experiments were conducted in a home-made continuous flow cell as shown in Figure 3.1. It is a three-compartment microfluidic cell consisting of a platinum foil as the counter electrode, a saturated Ag/AgCl reference electrode and two current collectors to deliver the electricity into the electrode. A Nafion membrane was used to separate

the electrolyte in the fluidic and anodic compartment. Two peristaltic pumps were used to circulate the electrolyte. The electrolyte was purged with argon for 30 min to eliminate any additional gases in the electrolyte. After the continuous flow cell was assembled, it was purged with CO_2 for 10 min at a flow rate of 20 mL/min to remove any other gases in the system.

Figure 3.1 Home-made flow cell assembled in a 3-compartment mode.

Constant potential electrolysis (CPE) was performed to determine how different factors affect the performance. The gas from the continuous flow cell for CO_2ERR was analysed using an online gas chromatograph (GC 7890B Agilent) at 10 min intervals. To analyse H_2 and CO concentrations concurrently, the GC features two columns (MolSieve 5A 60-80 mesh and HayeSep Q 80/100) and two thermo-conductivity detectors (TCD). The carrier gases were helium and argon, respectively.

The FE of CO was determined by Equation (1), where n_i and n_{i-1} are the amounts of CO produced between specific injections, Q_i and Q_{i-1} are the charges in the system at the corresponding time, n_e is the number of electrons transferred in the reaction which is 2 for CO_2 convert to CO, F is the Faraday's constant.

$$FE(CO) = \frac{(n_i - n_{i-1}) * n_e * F}{Q_i - Q_{i-1}} * 100\% \quad (1)$$

Solar-driven electrochemical experiments were also conducted in the continuous flow cell. A commercial silicon solar panel (Arlec 25W Solar Panel, two 12V DC sockets) and a light source (Arlec model HL10 serie7) were used. The solar panel can produce the highest voltage of 12V. The gas output from the continuous flow cell in the experiment was analysed by GC 2014 Shimadzu. The column used was ShinCarbon ST 80/100. The carrier gas was argon.

Chapter 4 Results and Discussion

4.1 Effect of the applied potentials on the CO_2ERR performance

To determine the suitable potential applied to the system achieving a higher FE_{CO}, the potentials ranging from -1.05V to -1.35V vs. NHE were applied for the CO_2ERR. Figure 4.1 depicts the FE_{CO} under different potential conditions over 1 h. The highest FE trend was obtained at the applied potential of -1.25V vs. NHE, representing the most suitable working potential for CO_2ERR. The cases with -1.05V vs. NHE and -1.35V vs. NHE are unlikely to produce any CO. A FE_{CO} of around 38 % was achieved at -1.15V vs. NHE.

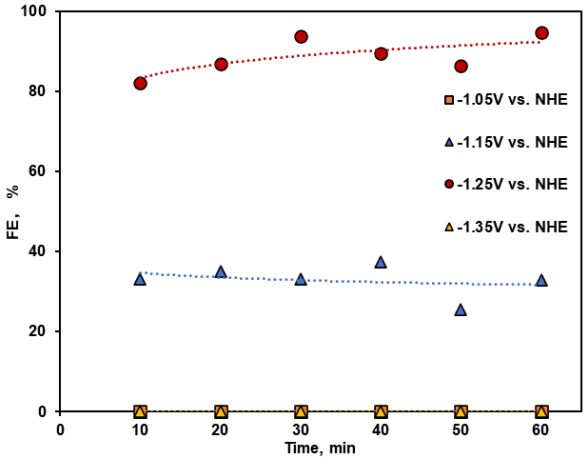

Figure 4.1 FE of CO over 1 h under the condition of 7 M KOH electrolyte, CoPc/CNTs catalyst loading of 1 mg/cm^2, a CO_2 flow rate of 40 mL/min with a reserved assembly electrochemical cell under -1.05V vs. NHE, -1.15V vs. NHE, -1.25V vs. NHE and -1.35V vs. NHE.

4.2 Effect of the CO_2 flow rates on the CO_2ERR performance

The FE_{CO} also depends on the CO_2 flow rate used in the system.[55] Higher flow rates facilitate a higher conversion rate of CO_2 to CO.[56, 57] However, the high flow rates reduce the reaction time of CO_2 to CO in the electrochemical cell, resulting in less CO_2 can be reduced each time when it passes the electrochemical cell [58, 59]. Therefore, it is crucial to determine the most suitable flow rate for the system. The effect of constant

CO_2 flow rates on the FE_{CO} is shown in Figure 4.2. Figure 4.2a shows that the FE_{CO} fell in 82-95 % in 1 h at a constant CO_2 flow rate of 40 mL/min. However, the instability of FE_{CO} indicates that the flow rate of 40 mL/min is not a suitable choice. At a flow rate of 30 mL/min as shown in Figure 4.2b, FE_{CO} kept decreasing, which corresponds well with the results from Esiner et al.[26]. This indicates that high flow rates are more likely to result in unstable FE_{CO}. As shown in Figure 4.2c, a much more stable FE_{CO} was obtained at 20 mL/min. While the FE_{CO} at 10 mL/min is much lower compared to that at 20 mL/min. Therefore, 20 mL/min was chosen as the most suitable flow rate for the following experiments.

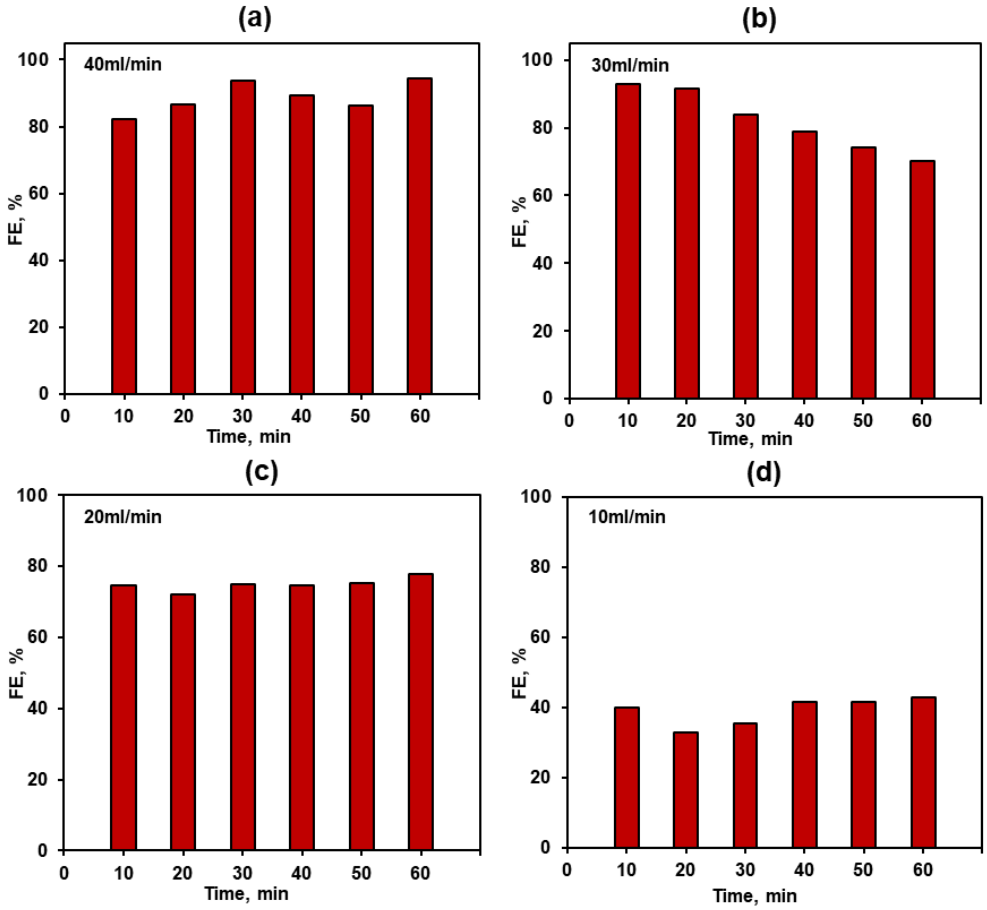

Figure 4.2: FE_{CO} over 1 h under the condition of 7 M KOH electrolyte and CoPc/CNTs catalyst loading of 1mg/cm^2 with a reserved assembly electrochemical cell under 1.25V vs. NHE at a CO_2 flow rate of (a) 40mL/min, (b) 30mL/min, (c) 20mL/min, and (d) 10mL/min.

4.3 Effect of different electrolyte on the CO_2ERR performance

Another important component of the CO_2ERR is the electrolyte, which enables to transfer electrons and protons between electrodes. The selection of a proper electrolyte is critical for the CO_2ERR.[60] Figure 4.3 compares the FE_{CO} when 0.5 M $KHCO_3$ and 7 M KOH were used as the electrolytes. The FE_{CO} of 89 % when using 0.5M $KHCO_3$ is much higher than that using 7M KOH. The higher the pH value, the more HCO_3^- and CO_3^- are accessible during the CO_2ERR[55], which means there is less chance for CO_2 to be converted to CO. A lower pH value when using 0.5M $KHCO_3$ resulted in a higher FE_{CO} compared with that of 7M KOH which presents a higher pH value. Therefore, 0.5M $KHCO_3$ was selected as the suitable electrolyte in the following experiments.

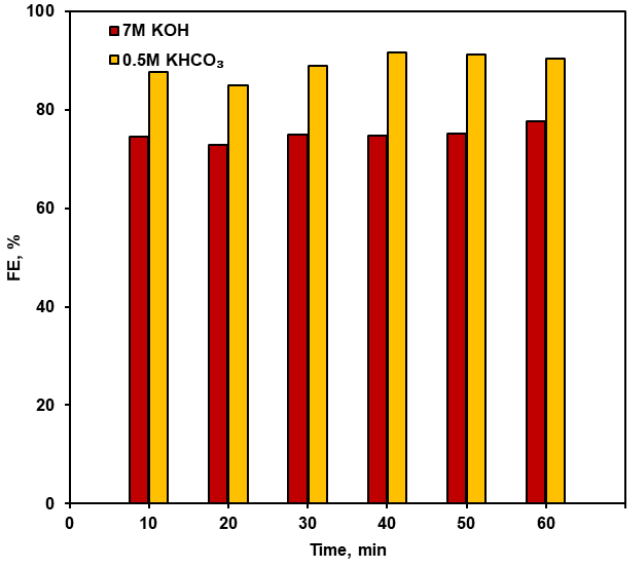

Figure 4.3 FE_{CO} using the electrolyte of 0.5M $KHCO_3$ (a) and KOH (b). CO_2ERR conditions: CoPc/CNTs catalyst loading of 1mg/cm^2, CO_2 flow rate of 20 mL/min, reserved assembly electrochemical cell under -1.25V vs. NHE, 1 h.

4.4 Effect of assembly methods on the CO_2ERR performance

Commonly, there are two assembly configurations for a continuous flow cell. As depicted in Figure 4.4a-b for reversed assembly, the PTFE microporous layer is faced with the electrolyte in the fluidic compartment, and the carbon layer is faced with the

CO_2 fed in the cathodic compartment. Figure 4.4c-d demonstrates the standard assembly, where the PTFE microporous layer faces with CO_2 and the carbon layer face with electrolyte. Cheng et al. reported that when the electrochemical cell is in reversed assembly, it can prevent flooding.[31] It appears that the electrochemical cell with reversed assembly can operate for a longer term.

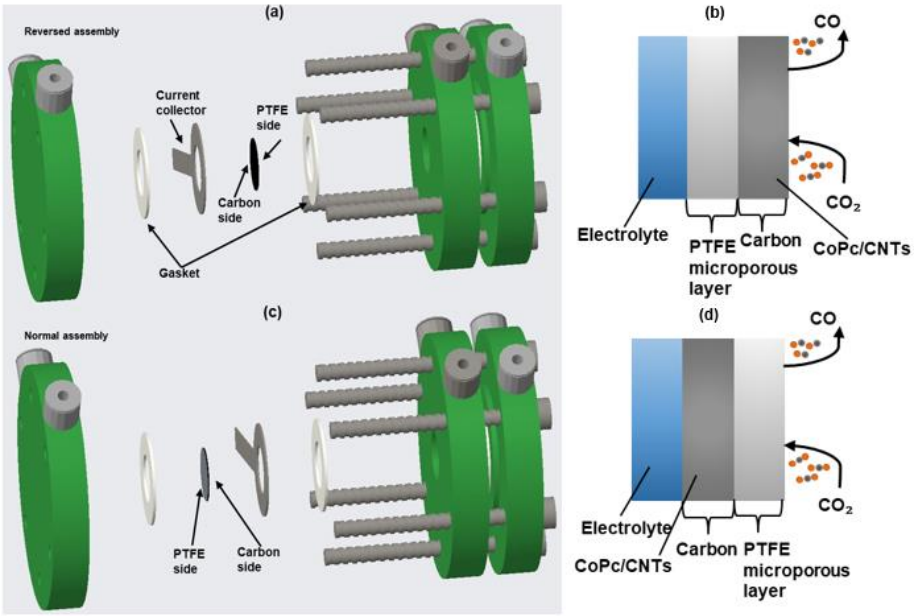

Figure 4.4: Schematic diagram of electrode configuration in reversed assembly (a-b); and in standard assembly (c-d).

The effects of the reversed and standard assembly on the FE_{CO} were investigated. Figure 4.5 compares the FE_{CO} of the two assembly methods in a 60-min CO_2ERR. It is apparent that the reversed assembly is in favour of the CO_2ERR. The average FE_{CO} is ca. 90 % in the reversed assembly, which is 14 % higher than that in the standard assembly. An earlier study by Cheng et al. [31] also reported that the reversed assembly has a better performance than the standard assembly, which aligns well with our findings. Therefore, the reversed assembly was chosen as the more suitable assembly method for all the experiments.

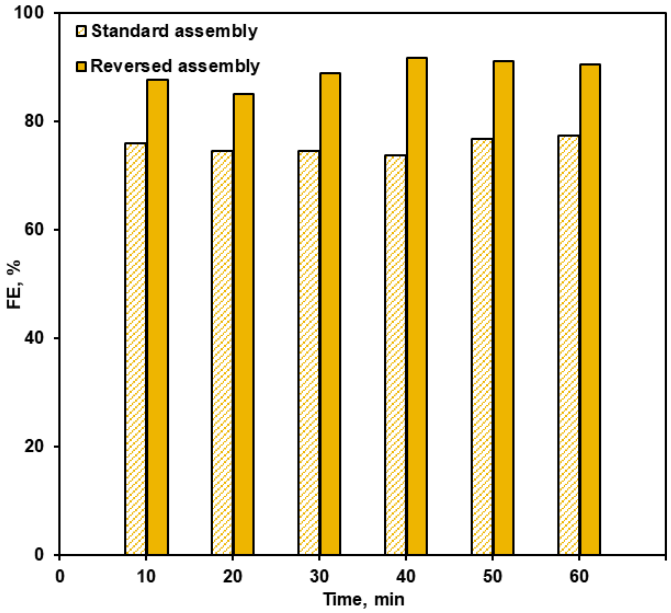

Figure 4.5: FE_{CO} with standard and reversed assembly. CO_2ERR conditions: CoPc/CNTs catalyst loading of 1mg/cm^2, CO_2 flow rate of 20 mL/min, under a potential of -1.25V vs. NHE, 1 h.

4.5 Long-term CO_2ERR performance

Long-term steady operation is essential for the practical use of flow reactors. Figure 4.6 shows the long-term CO_2ERR experiment under the optimal potential (-1.25V vs. NHE), constant CO_2 flow rate (20 mL/min), 0.5M $KHCO_3$ electrolyte, and reversed assembly. The achieved FE_{CO} is high and relatively stable over 4 h. This corresponds well with the finding from Zhang et al.[61].

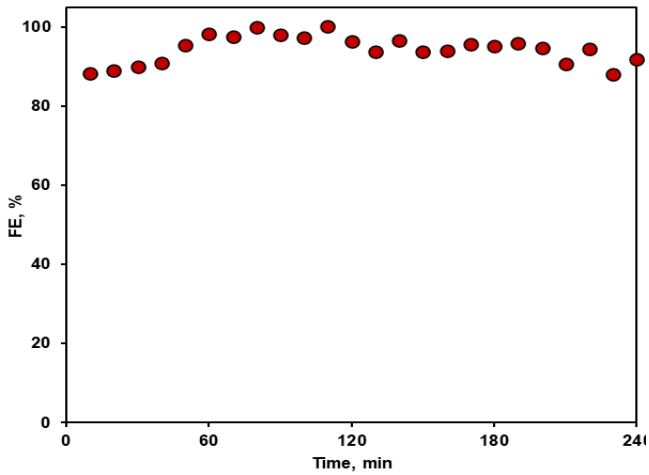

Figure 4.6: FE_{CO} of the long-term CO_2ERR experiment und the conditions: CoPc/CNTs

catalyst loading of 1mg/cm^2, CO_2 flow rate of 20 mL/min, under a potential of -1.25V vs. NHE, 4 h.

4.6 Design and evaluation of PV-EC integrated CO_2ERR system

A PV-EC integrated CO_2ERR system was designed to operate at a desirable potential. Figure 4.7 demonstrates the proposed configuration for the integrated PV-EC system for CO_2ERR. After the solar panel, a potential divider and Zener diode was added, acting as the voltage regulator. As such, the output potential of the solar cell matches the proper operating potential for the electrochemical cell. The value of the Zener diode used here was chosen as 3.6 V as the most suitable cell voltage obtained from the earlier experiment on the optimal potential of -1.25V vs. NHE. The 10μF capacitor here was used as a stabiliser to filter the AC. Since the current passing through the electrochemical cell cannot be measured directly from the potentiostat when doing the CO_2ERR with the integrated system, a shunt resistor connected in series with the electrochemical cell was used to measure the voltage obtained and calculate the value of the current passing through the electrochemical cell by Ohm's law. The shunt resistor itself has a very low resistance of only about 0.0956Ω. The much lower resistance compared with the resistance of the electrochemical cell means the shunt resistor did not take much potential from the system.

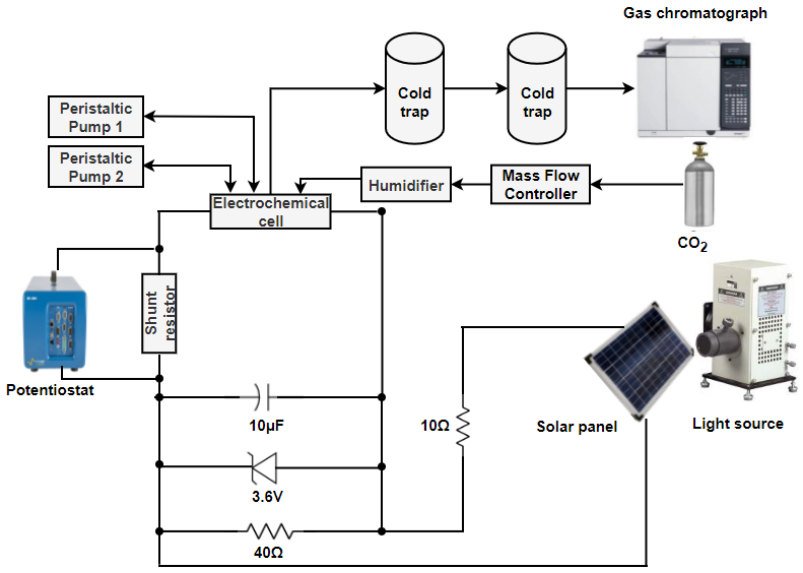

Figure 4.7: Schematic diagram of the integrated PV-EC system

Figure 4.8 compares the FE_{CO} obtained at two different potentials 3.4 V and 3.8V applied to the electrochemical cell when using the PV-EC integrated system. 3.4 V is the highest potential that can be reached without the voltage regulator, whereas 3.8 V is the best potential for working electrode (-1.25V vs. NHE) provided with the voltage regulator. It is apparent that the average FE_{CO} of 58 % under 3.8V is higher than that (47 %) under 3.4V.

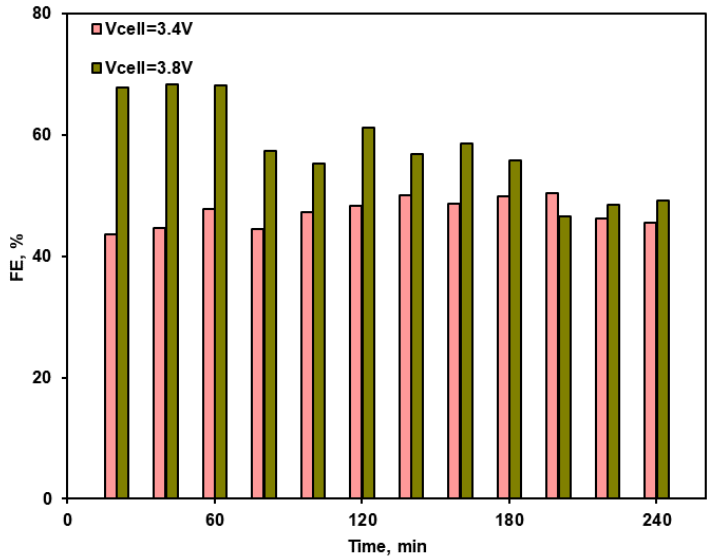

Figure 4.8: Long-term experiment of FE_{CO} obtained the CO_2ERR conducted in an integrated PV-EC system under 3.4V and 3.8V, respectively under the conditions: CoPc/CNTs catalyst loading of 1mg/cm^2, CO_2 flow rate of 10 mL/min, under a voltage of 3.4 V and 3.8 V, 4 h.

Chapter 5 Conclusions and future work

The different factor affecting the performance is investigated in this work. From the above observations, the most suitable potential is -1.25V vs. NHE. The potential significantly impacts the FE_{CO} performance and stability. CO_2 flow rate determines the conversion rate for CO_2 to CO. The system's most suitable constant flow rate input is 20 mL/min. When the flow rate is too high and too low, it causes low-single pass reduction, and the formulation productions contain lesser CO and more H_2, respectively. The choice of electrolytes and assembly methods has a significant impact on the CO_2ERR performance and stability. The results show that using 0.5M $KHCO_3$ and assembled reversely leads to a higher FE_{CO} and relative stability. A FE_{CO} of 90 % was achieved in the long-term CO_2ERR experiment operating under the optimal parameters. Furthermore, this thesis also presents the design of a proposed PV-EC integrated system and tested for the CO_2ERR under two potentials (3.4 V and 3.8 V). It was found that the average FE_{CO} obtained at 3.8V is higher than that at 3.4 V. The stability of the CO_2ERR performance operated in the PV-EC integrated system still needs further improvement in the future work. One of the main factors that may improve the stability is to develop a more stable electrocatalyst. Improving catalyst stability is critical for a practical CO_2ERR system. Another point for optimising the CO_2ERR system is to decrease the overpotential for the reduction reaction. A low overpotential and high CO_2 concentration could reduce CO_2 losses. In addition, the coupling method of the PV-EC system also needs to be considered or CO_2ERR. For example, although a DC-DC converter can reach the maximum power output of a solar cell, it has an actual energy loss of about 5–10 % [62]. Similarly, the voltage regulator component reported in this work also partially consumes the electricity passed to the electrochemical cell. This can explain why there is a drop in the FE_{CO} in the designed PV-EC system compared to that in the EC component itself. Therefore, it is very important to optimise the electrical setup in the system to minimise the energy loss in the future work.

References

1. Rosa, L. P.; Tolmasquim, M. T., An analytical model to compare energy-efficiency indices and CO_2 emissions in developed and developing countries. *Energy Policy* **1993,** *21* (3), 276-283.
2. Wolsky, A. M.; Daniels, E. J.; Jody, B. J., CO_2 capture from the flue gas of conventional fossil-fuel-fired power plants. *Environ. Prog.* **1994,** *13* (3), 214-219.
3. Yeh, A. C.; Bai, H., Comparison of ammonia and monoethanolamine solvents to reduce CO_2 greenhouse gas emissions. *Sci. Total Environ.* **1999,** *228* (2), 121-133.
4. Chauvy, R.; Meunier, N.; Thomas, D.; De Weireld, G., Selecting emerging CO_2 utilisation products for short-to mid-term deployment. *Appl. Energy* **2019,** *236*, 662-680.
5. Ghiat, I.; Al-Ansari, T., A review of carbon capture and utilisation as a CO_2 abatement opportunity within the EWF nexus. *J. CO_2 Util.* **2021,** *45*, 101432.
6. Schlesinger, M. D.; Benson, H. E.; Murphy, E. M.; Storch, H. H., Chemicals from the Fischer-Tropsch Synthesis. *Ind. Eng. Chem.* **1954,** *46* (6), 1322-1326.
7. Liu, Y.; Murata, K.; Inaba, M.; Takahara, I., Synthesis of ethanol from methanol and syngas through an indirect route containing methanol dehydrogenation, DME carbonylation, and methyl acetate hydrogenolysis. *Fuel Process. Technol.* **2013,** *110*, 206-213.
8. Jin, D.; Zhu, B.; Hou, Z.; Fei, J.; Lou, H.; Zheng, X., Dimethyl ether synthesis via methanol and syngas over rare earth metals modified zeolite Y and dual Cu–Mn–Zn catalysts. *Fuel* **2007,** *86* (17), 2707-2713.
9. He, J.; Janáky, C., Recent Advances in Solar-Driven Carbon Dioxide Conversion: Expectations versus Reality. *ACS Energy Lett.* **2020,** *5* (6), 1996-2014.
10. Wu, J.; Huang, Y.; Ye, W.; Li, Y., CO_2 Reduction: From the Electrochemical to Photochemical Approach. *Adv. Sci.* **2017,** *4* (11), 1700194.
11. Rong, Y.; Hu, Y.; Mei, A.; Tan, H.; Saidaminov, M. I.; Seok, S. I.; McGehee, M. D.; Sargent, E. H.; Han, H., Challenges for commercialising perovskite solar cells. *Science* **2018,** *361* (6408), eaat8235.
12. Zhang, J.; Gao, X.; Deng, Y.; Zha, Y.; Yuan, C., Comparison of life cycle environmental impacts of different perovskite solar cell systems. *Sol. Energy Mater. Sol. Cells* **2017,** *166*, 9-17.
13. Pérez-Rodríguez, S.; Barreras, F.; Pastor, E.; Lázaro, M. J., Electrochemical reactors for CO_2 reduction: From acid media to gas phase. *Int. J. Hydrogen Energy* **2016,** *41* (43), 19756-19765.
14. Vermaas, D. A.; Smith, W. A., Synergistic Electrochemical CO_2 Reduction and Water Oxidation with a Bipolar Membrane. *ACS Energy Lett.* **2016,** *1* (6), 1143-1148.
15. Becker, C.; Amkreutz, D.; Sontheimer, T.; Preidel, V.; Lockau, D.; Haschke, J.; Jogschies, L.; Klimm, C.; Merkel, J. J.; Plocica, P.; Steffens, S.; Rech, B., Polycrystalline silicon thin-film solar cells: Status and perspectives. *Sol. Energy Mater. Sol. Cells* **2013,** *119*, 112-123.
16. Sultan, S.; Hyun Kim, J.; Kim, S.; Kwon, Y.; Sung Lee, J., Innovative strategies toward challenges in PV-powered electrochemical CO_2 reduction. *J. Energy*

Chem. **2021,** *60*, 410-416.
17. Sriramagiri, G. M.; Ahmed, N.; Luc, W.; Dobson, K. D.; Hegedus, S. S.; Jiao, F., Toward a Practical Solar-Driven CO_2 Flow Cell Electrolyzer: Design and Optimisation. *ACS Sustain. Chem. Eng.* **2017,** *5* (11), 10959-10966.
18. Chae, S. Y.; Lee, S. Y.; Han, S. G.; Kim, H.; Ko, J.; Park, S.; Joo, O.-S.; Kim, D.; Kang, Y.; Lee, U.; Hwang, Y. J.; Min, B. K., A perspective on practical solar to carbon monoxide production devices with economic evaluation. *Sustain. Energy Fuels* **2020,** *4* (1), 199-212.
19. Sriramagiri, Gowri M.; Luc, W.; Jiao, F.; Ayers, K.; Dobson, K. D.; Hegedus, S. S., Computation and assessment of solar electrolyser field performance: comparing coupling strategies. *Sustain. Energy Fuels* **2019,** *3* (2), 422-430.
20. Arai, T.; Sato, S.; Sekizawa, K.; Suzuki, T. M.; Morikawa, T., Solar-driven CO_2 to CO reduction utilising H_2O as an electron donor by earth-abundant Mn–bipyridine complex and Ni-modified Fe-oxyhydroxide catalysts activated in a single-compartment reactor. *Chem. Commun.* **2019,** *55* (2), 237-240.
21. Ghausi, M. A.; Xie, J.; Li, Q.; Wang, X.; Yang, R.; Wu, M.; Wang, Y.; Dai, L., CO_2 Overall Splitting by a Bifunctional Metal-Free Electrocatalyst. *Angew. Chem. Int. Ed.* **2018,** *57* (40), 13135-13139.
22. Asadi, M.; Kim, K.; Liu, C.; Addepalli, A. V.; Abbasi, P.; Yasaei, P.; Phillips, P.; Behranginia, A.; Cerrato, J. M.; Haasch, R.; Zapol, P.; Kumar, B.; Klie, R. F.; Abiade, J.; Curtiss, L. A.; Salehi-Khojin, A., Nanostructured transition metal dichalcogenide electrocatalysts for CO_2 reduction in ionic liquid. *Science* **2016,** *353* (6298), 467.
23. Urbain, F.; Tang, P.; Carretero, N. M.; Andreu, T.; Gerling, L. G.; Voz, C.; Arbiol, J.; Morante, J. R., A prototype reactor for highly selective solar-driven CO_2 reduction to synthesis gas using nanosized earth-abundant catalysts and silicon photovoltaics. *Energy Environ. Sci.* **2017,** *10* (10), 2256-2266.
24. Deng, W.; Zhang, L.; Dong, H.; Chang, X.; Wang, T.; Gong, J., Achieving convenient CO_2 electroreduction and photovoltage in tandem using potential-insensitive disordered Ag nanoparticles. *Chem. Sci.* **2018,** *9* (32), 6599-6604.
25. Green, M. A.; Ho-Baillie, A.; Snaith, H. J., The emergence of perovskite solar cells. *Nat. Photonics* **2014,** *8* (7), 506-514.
26. Esiner, S.; Wang, J.; Janssen, R. A. J., Light-Driven Electrochemical Carbon Dioxide Reduction to Carbon Monoxide and Methane Using Perovskite Photovoltaics. *Cell Rep. Phys. Sci.* **2020,** *1* (5), 100058.
27. Schreier, M.; Curvat, L.; Giordano, F.; Steier, L.; Abate, A.; Zakeeruddin, S. M.; Luo, J.; Mayer, M. T.; Grätzel, M., Efficient photosynthesis of carbon monoxide from CO2 using perovskite photovoltaics. *Nat. Commun.* **2015,** *6* (1), 7326.
28. Jang, Y. J.; Jeong, I.; Lee, J.; Lee, J.; Ko, M. J.; Lee, J. S., Unbiased Sunlight-Driven Artificial Photosynthesis of Carbon Monoxide from CO_2 Using a ZnTe-Based Photocathode and a Perovskite Solar Cell in Tandem. *ACS Nano* **2016,** *10* (7), 6980-6987.
29. Kakavelakis, G.; Petridis, K.; Kymakis, E., Recent advances in plasmonic metal and rare-earth-element upconversion nanoparticle doped perovskite solar cells. *J.*

Mater. Chem. A **2017,** *5* (41), 21604-21624.
30. Wang, Y.; Liu, J.; Wang, Y.; Wang, Y.; Zheng, G., Efficient solar-driven electrocatalytic CO_2 reduction in a redox-medium-assisted system. *Nat. Commun.* **2018,** *9* (1), 5003.
31. Cheng, W.-H.; Richter, M. H.; Sullivan, I.; Larson, D. M.; Xiang, C.; Brunschwig, B. S.; Atwater, H. A., CO2 Reduction to CO with 19% Efficiency in a Solar-Driven Gas Diffusion Electrode Flow Cell under Outdoor Solar Illumination. *ACS Energy Lett.* **2020,** *5* (2), 470-476.
32. Schreier, M.; Héroguel, F.; Steier, L.; Ahmad, S.; Luterbacher, J. S.; Mayer, M. T.; Luo, J.; Grätzel, M., Solar conversion of CO_2 to CO using Earth-abundant electrocatalysts prepared by atomic layer modification of CuO. *Nat. Energy* **2017,** *2* (7), 17087.
33. Kim, B.; Seong, H.; Song, J. T.; Kwak, K.; Song, H.; Tan, Y. C.; Park, G.; Lee, D.; Oh, J., Over a 15.9% Solar-to-CO Conversion from Dilute CO_2 Streams Catalysed by Gold Nanoclusters Exhibiting a High CO_2 Binding Affinity. *ACS Energy Lett.* **2020,** *5* (3), 749-757.
34. Xiao, Y.; Qian, Y.; Chen, A.; Qin, T.; Zhang, F.; Tang, H.; Qiu, Z.; Lin, B.-L., An artificial photosynthetic system with CO_2-reducing solar-to-fuel efficiency exceeding 20%. *J. Mater. Chem. A* **2020,** *8* (35), 18310-18317.
35. Jiang, K.; Siahrostami, S.; Akey, A. J.; Li, Y.; Lu, Z.; Lattimer, J.; Hu, Y.; Stokes, C.; Gangishetty, M.; Chen, G.; Zhou, Y.; Hill, W.; Cai, W.-B.; Bell, D.; Chan, K.; Nørskov, J. K.; Cui, Y.; Wang, H., Transition-Metal Single Atoms in a Graphene Shell as Active Centers for Highly Efficient Artificial Photosynthesis. *Chem* **2017,** *3* (6), 950-960.
36. Zhou, L. Q.; Ling, C.; Zhou, H.; Wang, X.; Liao, J.; Reddy, G. K.; Deng, L.; Peck, T. C.; Zhang, R.; Whittingham, M. S.; Wang, C.; Chu, C.-W.; Yao, Y.; Jia, H., A high-performance oxygen evolution catalyst in neutral-pH for sunlight-driven CO_2 reduction. *Nat. Commun.* **2019,** *10* (1), 4081.
37. Mi, Y.; Qiu, Y.; Liu, Y.; Peng, X.; Hu, M.; Zhao, S.; Cao, H.; Zhuo, L.; Li, H.; Ren, J.; Liu, X.; Luo, J., Cobalt−Iron Oxide Nanosheets for High-Efficiency Solar-Driven CO_2−H_2O Coupling Electrocatalytic Reactions. *Adv. Funct. Mater.* **2020,** *30* (31), 2003438.
38. Wang, X.; Ghausi, M. A.; Yang, R.; Wu, M.; Xie, J.; Wang, Y., A photovoltaic-driven solid-state Zn–CO_2 electrochemical cell system with sunlight-insusceptible chemical production. *J. Mater. Chem. A* **2020,** *8* (27), 13806-13811.
39. Asadi, M.; Motevaselian, M. H.; Moradzadeh, A.; Majidi, L.; Esmaeilirad, M.; Sun, T. V.; Liu, C.; Bose, R.; Abbasi, P.; Zapol, P.; Khodadoust, A. P.; Curtiss, L. A.; Aluru, N. R.; Salehi-Khojin, A., Highly Efficient Solar-Driven Carbon Dioxide Reduction on Molybdenum Disulfide Catalyst Using Choline Chloride-Based Electrolyte. *Adv. Energy Mater.* **2019,** *9* (9), 1803536.
40. Liu, C.; Colón, B. C.; Ziesack, M.; Silver, P. A.; Nocera, D. G., Water splitting-biosynthetic system with CO_2 reduction efficiencies exceeding photosynthesis. *Science (Am. Assoc. Adv. Sci.)* **2016,** *352* (6290), 1210-1213.
41. Sacco, A.; Speranza, R.; Savino, U.; Zeng, J.; Farkhondehfal, M. A.;

Lamberti, A.; Chiodoni, A.; Pirri, C. F., An Integrated Device for the Solar-Driven Electrochemical Conversion of CO_2 to CO. *ACS Sustain. Chem. Eng.* **2020,** *8* (20), 7563-7568.
42. Xie, J.; Huang, Y.; Wu, M.; Wang, Y., Electrochemical Carbon Dioxide Splitting. *ChemElectroChem* **2019,** *6* (6), 1587-1604.
43. Zhou, X.; Liu, R.; Sun, K.; Chen, Y.; Verlage, E.; Francis, S. A.; Lewis, N. S.; Xiang, C., Solar-Driven Reduction of 1 atm of CO_2 to Formate at 10% Energy-Conversion Efficiency by Use of a TiO_2-Protected III–V Tandem Photoanode in Conjunction with a Bipolar Membrane and a Pd/C Cathode. *ACS Energy Lett.* **2016,** *1* (4), 764-770.
44. McDonald, M. B.; Ardo, S.; Lewis, N. S.; Freund, M. S., Use of Bipolar Membranes for Maintaining Steady-State pH Gradients in Membrane-Supported, Solar-Driven Water Splitting. *ChemSusChem* **2014,** *7* (11), 3021-3027.
45. Chabi, S.; Papadantonakis, K. M.; Lewis, N. S.; Freund, M. S., Membranes for artificial photosynthesis. *Energy Environ. Sci.* **2017,** *10* (6), 1320-1338.
46. Li, Y. C.; Zhou, D.; Yan, Z.; Gonçalves, R. H.; Salvatore, D. A.; Berlinguette, C. P.; Mallouk, T. E., Electrolysis of CO_2 to Syngas in Bipolar Membrane-Based Electrochemical Cells. *ACS Energy Lett.* **2016,** *1* (6), 1149-1153.
47. Verma, S.; Lu, X.; Ma, S.; Masel, R. I.; Kenis, P. J. A., The effect of electrolyte composition on the electroreduction of CO_2 to CO on Ag based gas diffusion electrodes. *Phys. Chem. Chem. Phys.* **2016,** *18* (10), 7075-7084.
48. Higgins, D.; Hahn, C.; Xiang, C.; Jaramillo, T. F.; Weber, A. Z., Gas-Diffusion Electrodes for Carbon Dioxide Reduction: A New Paradigm. *ACS Energy Lett.* **2019,** *4* (1), 317-324.
49. Singh, M. R.; Papadantonakis, K.; Xiang, C.; Lewis, N. S., An electrochemical engineering assessment of the operational conditions and constraints for solar-driven water-splitting systems at near-neutral pH. *Energy Environ. Sci.* **2015,** *8* (9), 2760-2767.
50. Lobaccaro, P.; Singh, M. R.; Clark, E. L.; Kwon, Y.; Bell, A. T.; Ager, J. W., Effects of temperature and gas–liquid mass transfer on the operation of small electrochemical cells for the quantitative evaluation of CO_2 reduction electrocatalysts. *Phys. Chem. Chem. Phys.* **2016,** *18* (38), 26777-26785.
51. Weng, L.-C.; Bell, A. T.; Weber, A. Z., Towards membrane-electrode assembly systems for CO_2 reduction: a modeling study. *Energy Environ. Sci.* **2019,** *12* (6), 1950-1968.
52. Song, J. T.; Song, H.; Kim, B.; Oh, J., Towards Higher Rate Electrochemical CO_2 Conversion: From Liquid-Phase to Gas-Phase Systems. *Catalysts* **2019,** *9* (3).
53. Li, J.; Chen, G.; Zhu, Y.; Liang, Z.; Pei, A.; Wu, C.-L.; Wang, H.; Lee, H. R.; Liu, K.; Chu, S.; Cui, Y., Efficient electrocatalytic CO_2 reduction on a three-phase interface. *Nat. Catal.* **2018,** *1* (8), 592-600.
54. Lide, D. R., *CRC handbook of chemistry and physics*. CRC press: 2004; Vol. 85.
55. Lees, E. W.; Mowbray, B. A. W.; Parlane, F. G. L.; Berlinguette, C. P., Gas diffusion electrodes and membranes for CO_2 reduction electrolysers. *Nat. Rev. Mater.* **2022,** *7* (1), 55-64.
56. Jeanty, P.; Scherer, C.; Magori, E.; Wiesner-Fleischer, K.; Hinrichsen, O.;

Fleischer, M., Upscaling and continuous operation of electrochemical CO_2 to CO conversion in aqueous solutions on silver gas diffusion electrodes. *J. CO_2 Util.* **2018,** *24*, 454-462.
57. Bhargava, S. S.; Proietto, F.; Azmoodeh, D.; Cofell, E. R.; Henckel, D. A.; Verma, S.; Brooks, C. J.; Gewirth, A. A.; Kenis, P. J. A., System Design Rules for Intensifying the Electrochemical Reduction of CO_2 to CO on Ag Nanoparticles. *ChemElectroChem* **2020,** *7* (9), 2001-2011.
58. Ripatti, D. S.; Veltman, T. R.; Kanan, M. W., Carbon Monoxide Gas Diffusion Electrolysis that Produces Concentrated C_2 Products with High Single-Pass Conversion. *Joule* **2019,** *3* (1), 240-256.
59. Jeng, E.; Jiao, F., Investigation of CO_2 single-pass conversion in a flow electrolyser. *React. Chem. Eng.* **2020,** *5* (9), 1768-1775.
60. Ma, D.; Jin, T.; Xie, K.; Huang, H., An overview of flow cell architecture design and optimisation for electrochemical CO_2 reduction. *J. Mater. Chem. A* **2021,** *9* (37), 20897-20918.
61. Zhang, X.; Wang, Y.; Gu, M.; Wang, M.; Zhang, Z.; Pan, W.; Jiang, Z.; Zheng, H.; Lucero, M.; Wang, H.; Sterbinsky, G. E.; Ma, Q.; Wang, Y.-G.; Feng, Z.; Li, J.; Dai, H.; Liang, Y., Molecular engineering of dispersed nickel phthalocyanines on carbon nanotubes for selective CO_2 reduction. *Nat. Energy* **2020,** *5* (9), 684-692.
62. Hossain, M. Z.; Rahim, N. A.; Selvaraj, J. a. l., Recent progress and development on power DC-DC converter topology, control, design and applications: A review. *Renew. Sust. Energ. Rev.* **2018,** *81*, 205-230.